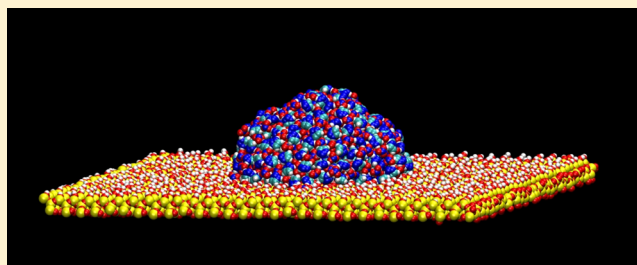


# Wetting and Tribological Properties of Ionic Liquids

Henry J. Castejón,\* Troy J. Wynn, and Zachary M. Marcin

Department of Chemistry, Wilkes University, Wilkes-Barre, Pennsylvania 18766, United States

**ABSTRACT:** A phenomenological study of the surface-wetting and tribological properties of various ionic liquids was conducted using molecular dynamics simulations. The surface-wetting capabilities of the liquids were studied by simulating the morphological transformation of an isolated liquid drop in vacuum to its equilibrium state on solid surface. The tribological properties of the liquids were probed examining their flow behaviors and viscosities in computational lubrication experiments. All liquids exhibited good surface-wetting properties, as demonstrated by the hemispherical shape of the droplets at equilibrium and the surface contact angles. Contact angles for all liquids were much lower than 90°. Lubrication experiments demonstrated a flow behavior for the liquids that depended on the magnitude of the applied shear rate. Three distinctive flow regimes were observed: Newtonian, thixotropic (non-Newtonian), and oversheared. The liquids' viscosities were determined in the Newtonian regime and agree well with experimental results and with previously reported values calculated using equilibrium simulations. The phenomenological approach implemented in this study allowed for the calculation of the transport properties of the liquids and produced values within the appropriate order of magnitude without the use of calculational artifacts. These results corroborate previous reports indicating that nonequilibrium techniques represent a more robust approach for the calculation of transport properties than do equilibrium methods based on time-correlation functions.



## INTRODUCTION

Although the most obvious application of ionic liquids is their use as electrolytes for batteries, due to their special properties, some unconventional applications have emerged, including suggestion of their use as lubricants. Current lubricants are mainly refined mineral oils, fluorinated polyethers, and polyol esters.<sup>1</sup> The great majority of these compounds are susceptible to catalytic degradation and display surface-wetting problems due to their high vapor pressures. Ionic liquids, on the other hand, are nonflammable, have negligible volatility, and have high thermal stability which could make them excellent lubricants. They have indeed been shown to exhibit excellent friction-reduction properties.<sup>2</sup> A study of the structure–property relationship of these liquids can allow for the design of ionic liquid lubricants with tailored capabilities.

The surface wetting properties of a liquid are determined by its ability to adhere to a surface. This ability is also important in many other industrial and scientific applications.<sup>3,4</sup> When a spherical liquid droplet is placed on a flat surface and equilibrium is attained, the shape of the drop resting on the surface depends on the molecular properties of the liquid drop, the air around it, and the material properties of the surface. This equilibrium state is described using Young's equation:<sup>5</sup>

$$\gamma_{SL} + \gamma \cos \theta = \gamma_{SV} \quad (1)$$

where the contact angle  $\theta$  is the angle between the air–liquid and surface–liquid interfaces, and  $\gamma_{SL}$ ,  $\gamma_{SV}$ , and  $\gamma$  are the surface tension between the solid and the liquid, the solid and the air, and the liquid and the air, respectively. Equation 1 can be

obtained from the application of equilibrium conditions to the thermodynamic work that is required for an incompressible liquid to expand its surface area. However, this one-dimensional analysis may not be sufficient to study the wetting properties of complex liquids (e.g., ionic liquids) due to their anisotropic properties. We will perform instead a fully three-dimensional analysis of the wetting process. Our analysis will incorporate the three-phase contact line (circumference line of the surface-drop area)<sup>6</sup> and will determine the spectrum of contact angles along the perimeter of the liquid–surface area enclosed by that three-phase contact line. To determine these angles, we will simulate the morphological transition that takes place when an ionic liquid goes from a spherical drop in the vacuum to a liquid droplet on top of a surface. Once the liquid has reached equilibrium on the surface, the contact angle will be measured by determining the phase boundaries in the system. A similar approach has been used to determine the contact angle of water on a silica surface.<sup>7</sup>

The lubricating capabilities of a liquid are dynamic properties. They are determined by the adhesion of the liquid to a surface in order to prevent surface wearing despite the presence of shear forces. To truly examine the lubricating capabilities of a liquid, it is necessary to study its behavior under the flow conditions that define the lubricating process.

**Received:** November 30, 2013

**Revised:** March 14, 2014

**Published:** March 17, 2014

In continuum mechanics the *lubrication approximation* is expressed as

$$\frac{\partial^2 v_x}{\partial z^2} = \frac{1}{\mu} \frac{dP}{dx}; \quad P = P(x) \quad (2)$$

which is the Navier–Stokes equation for an unidirectional, steady, viscous flow in a thin channel or narrow gap between two solid objects,<sup>8</sup> as it is schematically shown in Figure 1. This

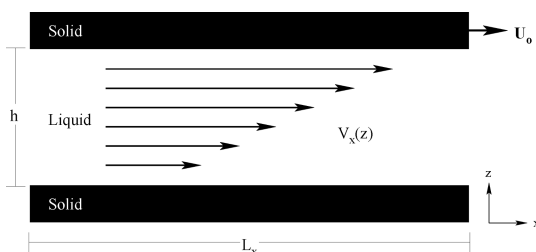


**Figure 1.** Schematic diagram of the lubricating process.

figure illustrates the precise tribological definition of lubrication: a liquid confined in between two solid surfaces in motion with respect to each other. Integration of eq 2 with the appropriate boundary conditions shows that the *lubrication approximation* depends on two fundamental conditions: one is geometrical and the other is dynamic. Application of the continuity equation<sup>9</sup> provides these two conditions for the system described above:

$$\frac{h}{L_x} \ll 1 \quad \text{and} \quad \left( \frac{\rho U h}{\mu} \right) \left( \frac{h}{L_x} \right) \ll 1 \quad (3)$$

The first is just a geometrical condition that obviously holds for thin films and channels like that one depicted in Figure 1. The second one is a dynamic condition that could be interpreted as the required commensurability between the ability of the liquid to be deformed and the speed at which it is spread on the surface. This is the more important condition. It can allow for the determination of the viscosity ( $\mu$ ) of the fluid. Here, we will again use a phenomenological approach. We will perform computer simulations under the same precise experimental conditions of the lubricating process in order to

determine the tribological properties of the liquids. The liquids will be placed in between two solid surfaces and allowed to equilibrate. Once at equilibrium, one surface will remain at rest while the other will slide at a constant velocity to generate a steady state. Then, the response of the system will be measured. A similar approach has been reported for liquid argon interacting via a short-range Lennard-Jones potential.<sup>10</sup> The use of a phenomenological approach prevents the unphysical fields sometimes created by pure mathematical approaches<sup>11</sup> and permits the direct use of the constitutive equations of transport phenomena.<sup>8</sup>

## METHODOLOGY

Classical molecular dynamics simulations were used to run *in silico* experiments in order to study the surface-wetting and lubricating capabilities of several ionic liquids in a phenomenological way. Wetting properties were examined by simulating the interaction of liquid droplets with a silica surface and observing their morphological transition into a liquid film on the surface. The lubricating capabilities of the liquids were then examined by a tribological experiment under the precise flow conditions that define the lubrication process. The liquids were placed between two solid surfaces, and to apply a shear force on the liquid, one of the surfaces was slid at a constant velocity while the other was kept stationary.

Simulations were performed using a locally modified version of GROMACS-4.5.<sup>12</sup> The program was modified to generate stationary nonequilibrium states, like the one depicted in Figure 1, and then impose a constant velocity on the top surface to generate a gradient of velocities across the bulk of the liquid. Molecular dynamics (MD) simulations were carried out using NVT and NPT ensembles appropriately (see Simulated Systems section). The cutoff of the Lennard-Jones and electrostatic interactions was taken as 10 Å. Long-range Coulombic interactions were treated using the particle mesh Ewald (PME) method with a Fourier grid spacing between 0.12 and 0.20 nm. The equations of motion were integrated using a leapfrog algorithm with an integration time of 0.5 fs. The temperature and the pressure were controlled using a Nosé–Hoover thermostat and a Parrinello–Rahman barostat with characteristic times of 0.5 and 2.0 ps, respectively. The barostat was set to a pressure of 1 bar, and the thermostat was set to the

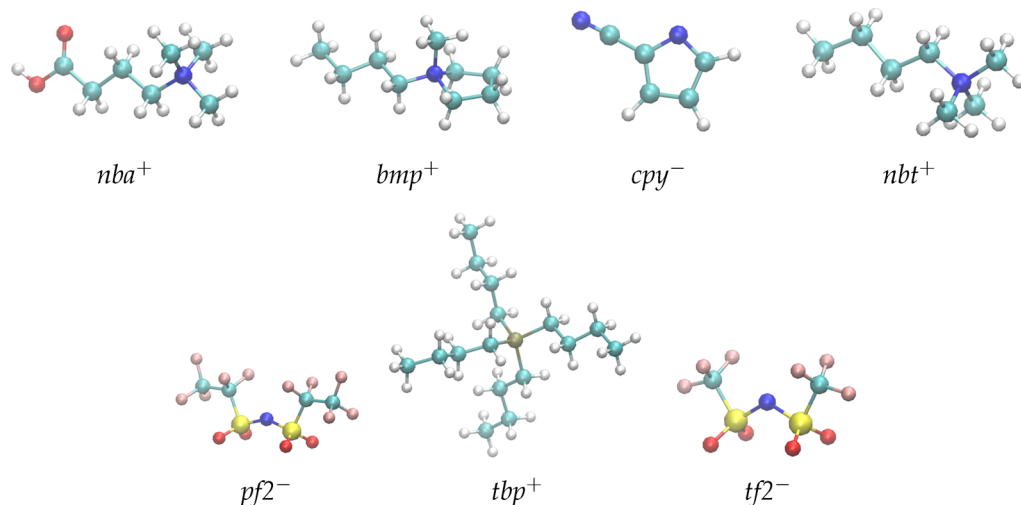


**Figure 2.** Simulated anions and cations.

temperature corresponding to the midpoint of liquid range of the respective system. Simulation temperatures ranged from 400 to 426 K for the liquids studied.

## SIMULATED SYSTEMS

Two types of systems were simulated: silica surfaces and ionic liquids. The silica surfaces were represented by quartz slabs generated by replicating a primitive unit cell of  $\alpha$ -quartz along the  $x$  and  $y$  directions to the desired dimensions. One face of the slab was terminated with silanol groups (Si-OH), the most common group on quartz surfaces.<sup>13</sup> This face is referred to as the silanol surface and constitutes the hydrophilic face of the silica slab. On the opposite face of the slab, which represented the hydrophobic surface, the silicon atoms were just hydrogenated to form silane groups. This surface is referred to as the silane surface. All interactions were represented using the CHARMM force field developed by MacKerell et al.<sup>14</sup> This force field was parametrized specifically for the quartz–water interface, a system in which the interactions are very similar to those present in this work. Bonded and nonbonded parameters in the force field were optimized using vibrational frequencies calculated quantum mechanically at the B3LYP/6-31G\* level of theory. The geometry of the quartz slabs was optimized in the presence of water to ensure the stability of the entire system.

The ionic liquids were generated by randomly inserting an equal number of cations and anions into a simulation box to form the desired liquid. The simulated liquids are 1-butyl-1-methylpyrrolidinium bis[(perfluoroethyl)sulfonyl]imide ([bmp][pf2]),  $N,N,N$ -trimethylammonium bis[(perfluoroethyl)sulfonyl]imide ([nba][pf2]),  $N$ -butyl- $N,N,N$ -trimethylammonium bis[(perfluoroethyl)sulfonyl]imide ([nbt][pf2]),  $N$ -butyl- $N,N,N$ -trimethylammonium bis[(trifluoromethyl)sulfonyl]imide ([nbt][tf2]), and tetrabutylphosphonium 2-cyanopyrrolide ([tbp][cpy]). The molecular structures of the cations and anions used are shown in Figure 2. For the wetting properties study, the total number of chemical species was 1000; for the tribological experiments, that number was increased to 2000 in order to collect better statistical data. Simulations for both wetting and tribological properties of one of the systems were run using twice the number of particles. Because the results were virtually identical, all simulations were performed using the smaller number of particles to increase computational efficiency.

The initial liquid configurations were equilibrated at the appropriate temperature and pressure until the experimental value of the liquid density was achieved. Intra- and intermolecular interactions were represented using nonpolarizable force-fields developed by Maginn et al.<sup>15,16</sup> with the functional form

$$V_{\text{total}} = \sum_{\text{bonds}} k_b(r - r_0)^2 + \sum_{\text{angles}} k_\theta(\theta - \theta_0)^2 + \sum_{\text{dihedrals}} k_\chi[1 + \cos(n\chi - \delta_\chi)] + \sum_{\text{improper}} k_\psi[1 + \cos(n\psi - \delta_\psi)] + \sum_{i=1}^{N-1} \sum_{j=i+1}^N \left\{ 4\epsilon_{ij} \left[ \left( \frac{\sigma_{ij}}{r_{ij}} \right)^{12} - \left( \frac{\sigma_{ij}}{r_{ij}} \right)^6 \right] + \frac{q_i q_j}{4\pi\epsilon_0 r_{ij}} \right\}$$

The first four summations represent the energy of the bonded interactions expressed in terms of bond stretching, angle bending, and dihedral and improper angle torsions. The last term represents the nonbonded interactions as Lennard-Jones potentials with a Coulombic component. These force fields were developed by carrying out *ab initio* molecular orbital (MO) calculations on the isolated ions to determine their optimized structures. The parametrization was done by performing geometry optimization scans at the Hartree–Fock level followed by single point calculations at the MP2/6-311+G(d,p) level of theory. The results from the MO calculations were then reproduced by doing molecular dynamics runs under the same geometrical constraints. The final parameters were obtained by fitting the energy profiles to the appropriate potential functions. The physical parameters utilized and studied in the development of these force fields included diffusion coefficients and shear viscosities, which makes them very suitable for the present simulations.

## RESULTS AND DISCUSSION

**Wetting Properties.** The silica wetting properties of the ionic liquids were studied by simulating the morphological transition of an isolated liquid drop in the vacuum to its equilibrium state on a silica surface. This equilibrium state was generally a hemispherical liquid droplet resting on top of the quartz surface. All final equilibrium states were realized by first equilibrating the cubic liquid drop and the silica surface separately. The drops were equilibrated at a temperature corresponding to the midpoint of liquid range of the ionic liquid and a pressure of 1 bar by using an NPT ensemble and ensuring that the density of the system corresponded to that of the experimental density of liquid used. The silica surface was represented as a quartz slab that was at a minimum 1.5 nm thick in order to prevent interaction of the two silica surfaces. The slab was equilibrated in a NVT ensemble at the same temperature of the liquid. Once both systems reached equilibrium, the liquid drop was placed on top of the quartz slab and allowed to evolve in time to a stationary state. Simulations were run until the systems reached a final geometrical configuration with a stationary contact angle. These configurations were generally achieved with runs of 5–7.5 ns. The degree of wetting was determined by measuring the contact angle of the liquid with the surface. This was done at two stages of the simulation. If both values agree within the standard deviation of each value, the system was considered to have reached the final equilibrium state. A sample of the final equilibrium state attained is shown in Figure 3. No substantial evaporation was observed during the equilibration runs: only a few liquid molecules drifted away from the bulk of the drop on the surface. All liquids equilibrated to drops with a quasi-hemispherical shape. The determination of the contact angles is shown schematically in Figure 4. The droplet boundaries were

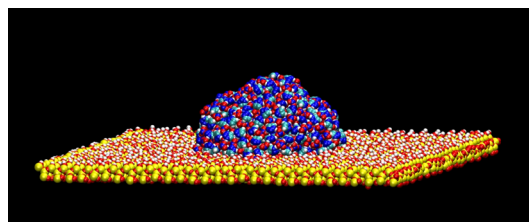


Figure 3. Liquid drop at equilibrium on quartz surface.



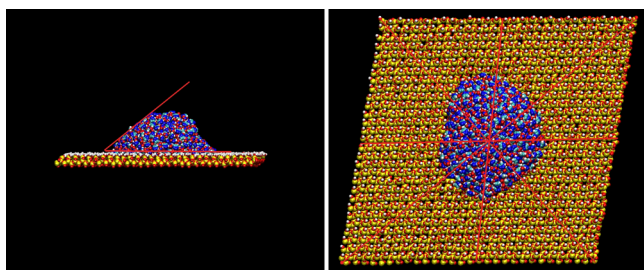


Figure 4. Determination of the liquid contact angle.

determined for adjacent horizontal layers of liquid, and the tangent line was traced. The contact angle was then determined as the angle between the horizontal line marking the liquid–surface interface and the line tangent to the droplet’s surface, as depicted in the left panel of Figure 4. Table 1 shows the contact

Table 1. Solid–Liquid Contact Angles (deg) on Quartz Surfaces

liquid	silanol surface	silane surface
[bmp][pf <sub>2</sub> ]	40.13 ± 5.17	45.38 ± 4.52
[cpy][tbp]	47.38 ± 11.66	56.0 ± 7.8
[nba][pf <sub>2</sub> ]	50.13 ± 19.12	55.13 ± 6.24
[nbt][pf <sub>2</sub> ]	37.63 ± 9.39	42.88 ± 4.85
[nbt][tf <sub>2</sub> ]	43.63 ± 6.28	41.38 ± 5.40

angles for all examined liquids on silanol and silane surfaces. All liquids displayed contact angles lower than 90°, which indicates a favorable liquid–surface interaction. Contact angles on the silanol surface are generally slightly lower than those on the silane surface. This may be an indication of the hydrophilicity difference of these two surfaces. This general trend in the magnitude of the wetting angles (i.e., they are always lower than 90°) suggests that these liquids may display laminar flow behavior under Couette flow conditions. Advancing contact angles were determined along four different directions on the solid surface (see right panel of Figure 4) in order to examine the effect of the crystallographic direction and surface packing on the spreading of the liquid. The spectrum of contact angles, rather than a single angle, can demonstrate the effect of the *local structure* on the liquid–surface interaction. Table 2 shows the advancing contact angles along four different directions on the surface for [bmp][pf<sub>2</sub>]. All the other liquids showed similar results; however, [bmp][pf<sub>2</sub>] displayed the lower standard deviation in the angles. The magnitude of the contact angles does not seem to change significantly with the crystallographic direction in which the liquid is advancing. Some studies have shown that dimensional and structural commensurability between the fluid and the solid surface lowers the contact angles.<sup>17</sup> It is possible that the molecular size of the ions in these liquids obscures the specific liquid–surface interactions in every crystallographic direction on the surface and diminishes their influence on the advance of the fluid. Consequently, the

crystallographic direction and the magnitude of the contact angles show no correlation.

#### Tribological Properties. Stationary Equilibrium States.

The computational experiment performed here replicates the precise tribological conditions of the lubrication process. It begins with the equilibrated system shown in Figure 5. This

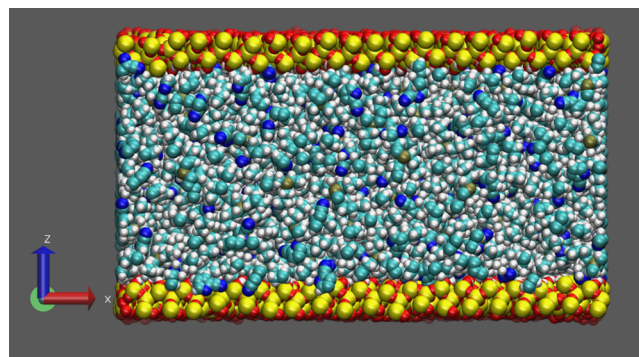


Figure 5. Static equilibrium state of the liquid confined in between two silica slabs.

figure depicts the ionic liquid confined in between two stationary silica slabs at thermodynamic equilibrium. Figure 6

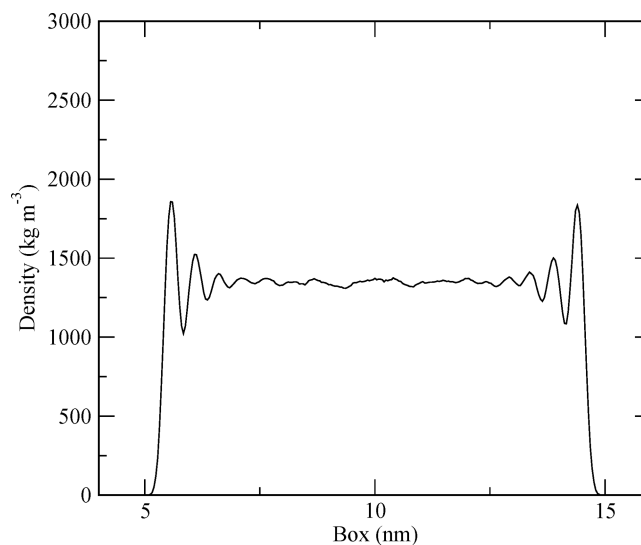


Figure 6. Typical density profile of the liquid in the *z*-direction.

shows the typical time-averaged density profile of the liquid along the *z*-direction in the static equilibrium. It can be observed how the interaction with the orderly surface induces the formation of structural features in the liquid. The liquid density oscillates along the direction perpendicular to the solid surfaces, and it reaches the highest values near the surface. This ordering is induced in the liquid by its interaction with the orderly structure of the silica surface. The density gradually

Table 2. Contact Angles (deg) for bmp-pf<sub>2</sub> on the Quartz Surfaces

surface	direction			
	0°	45°	90°	135°
silanol	45.00 ± 1.00	47.00 ± 1.00	38.50 ± 5.50	39.00 ± 4.00
silane	45.00 ± 5.00	41.00 ± 0.50	45.75 ± 2.75	49.75 ± 0.25

decays on going away from the surface until reaching the bulk density of the liquid. The strength of the surface–liquid interaction determines the magnitude of the density peaks and their gradual decay. This behavior, which corroborates the wetting results obtained in the previous section, has been observed in ionic liquids confined inside nanopores<sup>18</sup> and simple Lennard-Jones liquids interacting with solid surfaces.<sup>19</sup> The static structure factor,  $S(\vec{k})$ , can provide more quantitative information about the ordering observed in the confined liquid.  $S(\vec{k})$  is calculated as

$$S(\vec{k}) = \left\langle \frac{1}{N_j} \left| \sum_j e^{i\vec{k} \cdot \vec{r}_j} \right|^2 \right\rangle \quad (4)$$

where  $N_j$  is the number of molecules (instead of atoms in order to avoid intramolecular peaks in the radial distribution function). The angular brackets denote an ensemble average. The static structure factor for the confined and nonconfined liquid is shown in Figure 7. The inset figure shows the sharp

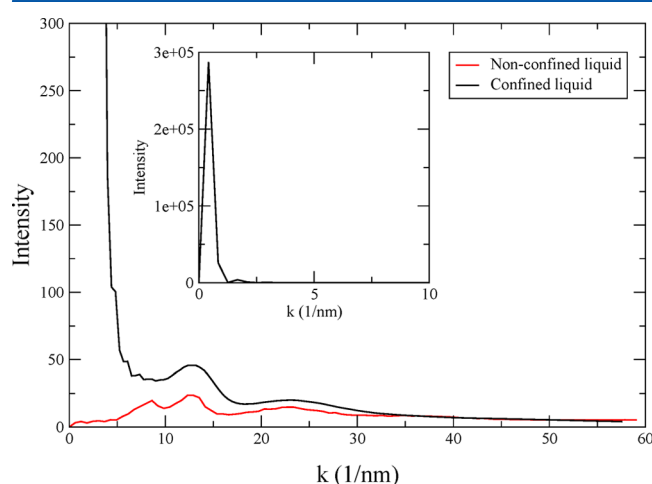


**Figure 7.** Static structure factors for the confined and nonconfined liquid.

peak obtained for the confined liquid. This peak suggests some weak ordering of the liquid in the  $xy$ -planes. Studies in simple liquids<sup>19</sup> have shown that this ordering corresponds to the formation of epitaxial layers with low-density areas in between them, yielding a structure that mimics that of the solid slab. These layers can, in turn, slide past each other easily, affecting the lubrication properties of the liquid. All the liquids studied here showed peaks in their density profiles near the solid surfaces. The ordering of the liquid structure in that region indicates their strong liquid–surface interaction which is consistent with the low contact angles found for all these liquids. The density profile along the  $z$ -axis, the magnitude of the density peaks, and the decay of the density toward the bulk of the liquid were also similar for all the liquids, which suggests a similar ordering. Studies have shown how solid surfaces induce structure in adjacent liquids and how this structuring can affect the momentum transfer in the liquid.<sup>20</sup>

**Stationary Nonequilibrium States.** The tribological experiment begins by sliding the upper surface in the  $x$ -direction at a uniform velocity ( $U_0$ ) until the system reaches a non-equilibrium steady state with a velocity profile as depicted in Figure 1. The sliding velocities ranged between 0.01 and 5.0

nm/ps, which corresponds to 10–5000 m/s. These sliding velocities also correspond to shear rates commonly used in engineering applications of Couette and Poiseuille flows,<sup>21</sup> and their range was sufficient to obtain the different flow behaviors typically observed in liquids under shear conditions. Figure 8

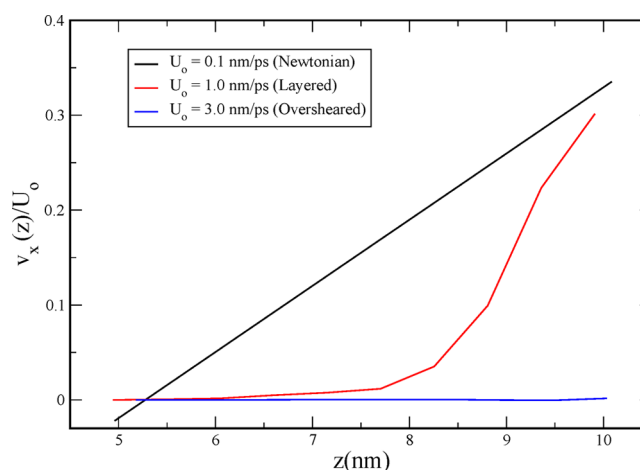


**Figure 8.** Typical flow regimes observed for all liquids.

shows the three different velocity gradients observed for all the liquids as the sliding velocity of the upper slab was varied. This figure shows a Newtonian flow behavior, represented by the linear velocity profile; a Non-Newtonian flow behavior, represented by the nonlinear velocity profile; and an oversheared flow, represented by the horizontal or flat velocity profile. The flow regimes observed correspond to the typical behavior of a liquid under shear conditions. At low shear, typically at a sliding velocity below 0.1 nm/ps, the liquid–surface interaction is sufficiently strong to transfer momentum efficiently. The viscosity of the liquid allows its deformation in the same time scale of the applied stress, causing a linear velocity profile or constant viscosity. Above the sliding velocity of 0.1 nm/ps, the liquid deformation is no longer synchronous with the shear applied, and the dragging force (i.e., momentum) is not transmitted efficiently. The liquid lags behind the moving slab at a velocity that decays with the distance. At an even higher sliding velocity (around 3.0 nm/ps), the strong liquid–surface interaction and the viscous interactions in the liquid are overwhelmed by the breaking of the inertia due to the rapid movement of the slab, and the liquid neither deforms in time nor keeps its bond with the surface in motion, but instead it lags behind completely oversheared. The appearance of the non-Newtonian behavior curve suggests that these liquids may have different static and flow structures.

Order parameters can provide a measure of the symmetry and order in a system. The order parameter  $S_z$ , which is calculated as

$$S_z = \frac{3}{2} \langle \cos^2 \theta_z \rangle - \frac{1}{2} \quad (5)$$

can provide information about the ordering and orientation of the liquid molecules. In eq 5,  $\theta_z$  is the angle between the  $z$ -axis of the system and the vector from  $C_{n-1}$  to  $C_{n+1}$  for the  $\text{CH}_2$  segments of the molecular species. A value of 1 indicates alignment with the  $z$ -axis (i.e., is perpendicular to the flow), whereas a value of  $-1/2$  indicates an alignment with the flow

direction. Table 3 shows the order parameter ( $S_z$ ) for the cationic species in the liquids. These species are the ones

**Table 3. Order Parameter for the Cationic Species in the Liquids**

liquid	static state	flow state		
	average	average	top	bottom
[bmp][pf <sub>2</sub> ]	0.2956	0.2959	0.3026	0.3722
[cpy][tbp]	0.2978	0.2996	0.2994	0.3007
[nba][pf <sub>2</sub> ]	0.3191	0.3185	0.3191	0.3203
[nbt][pf <sub>2</sub> ]	0.3244	0.3222	0.3221	0.3357
[nbt][tf <sub>2</sub> ]	0.3222	0.3178	0.3240	0.3220

containing CH<sub>2</sub> segments. The anions are mainly rigid rings or short quasi-spherical molecules that do not undergo much deformation under flow conditions. In the static equilibrium state (column 1), most species display values that indicate a random or quasi-random orientation. No significant differences are observed when comparing the order parameter of the static equilibrium state with the average value of  $S_z$  in the flow state. However, when the order parameter for the flow state is partitioned into the averages values for the top and bottom layers in the system, some interesting results are obtained. Both average values (for the top and the bottom layers) are higher than the average value for the overall system. This may be due to the stronger interaction of the liquid in these layers, as compared with the liquid in the bulk, with the solid surface. This interaction, as shown in previous sections, induces some orientation in the liquid. When comparing the order parameters for the top and bottom layers, the top layers, which are subjected to the higher shear stress, display a slightly lower order parameter. This indicates some aligning with the shear direction as the liquid flows. It may be possible to observe a more definite orientation in the liquid by inducing flow with direct pressure instead of shear stress.

Figure 9 shows the Newtonian behavior of all the liquids. In this regime, the spreading of the liquid is commensurate with

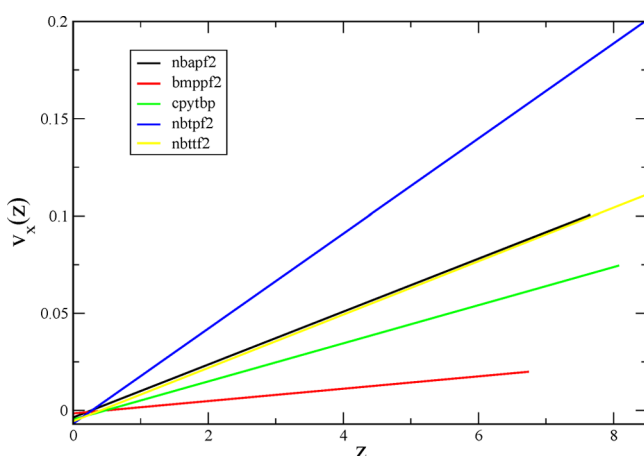


**Figure 9.** Newtonian behavior observed for all liquids.

shear rate applied, which yields a constant viscosity. In the Newtonian regime, the shear viscosity ( $\mu$ ) can be calculated from the microscopic stress tensor ( $\tau_{xz}$ ):

$$\tau_{xz} = \mu \left( \frac{\partial v_x}{\partial z} \right) \quad (6)$$

Table 4 shows the calculated shear viscosities along with some other tribological properties. The viscosities in the

**Table 4. Tribological Properties of the Liquids Studied**

liquid	viscosity (Pa·s)	sliding velocity (nm/ps)	slip length (nm)
[bmp][pf <sub>2</sub> ]	0.001 867	0.010	0.00
[cpy][tbp]	0.002 442	0.050	0.55
[nba][pf <sub>2</sub> ]	0.002 125	0.050	0.00
[nbt][pf <sub>2</sub> ]	0.001 098	0.050	0.26
[nbt][tf <sub>2</sub> ]	0.001 918	0.050	0.00

Newtonian-flow regimes were calculated using eq 6. Unlike equilibrium simulations<sup>15</sup> that have been shown to overestimate the experimental viscosities by up to 1 order of magnitude, the nonequilibrium approach used in this work yields values that are within the order of magnitude of the viscosities of similar liquids,<sup>15</sup> and the relative values of the viscosities display the correct trend. Namely, liquids composed of molecular species with long tails, bulky and oddly shaped ions, and polar functional groups display a higher viscosity than those composed of smaller, quasi-spherical and compact molecular species. The overestimation of the viscosities of ionic liquids by equilibrium calculations has been attributed to a slowing of the dynamics of the liquids due to the neglect of the polarizability in the force field.<sup>22,23</sup> Some studies,<sup>24</sup> however, have shown nonequilibrium methods to be a more robust approach to estimate shear viscosities than equilibrium techniques that use time autocorrelation functions. It is worth noticing that, in the calculation of transport properties, nonequilibrium techniques deal with the signal of the property being calculated, whereas equilibrium methods deal with the oscillations of the same signal at equilibrium.

Table 4 also shows the slip length for each simulated liquid. The slip distance was calculated using the linear Navier boundary condition:

$$\Delta V = \dot{\gamma} L_s \quad (7)$$

where  $\Delta V$  is the velocity difference between the slab and the adjacent liquid,  $\dot{\gamma}$  is the shear rate, and  $L_s$  is the slip length. This condition is only valid at low shear-rate regimes.<sup>25</sup>

The slip distance is an important property that can provide insights into the liquid–solid interaction and its effect on the liquid structure during the lubrication process. It is particularly important in nanoscale fluid mechanics; at the nanoscale level, liquids flowing through channels can encounter large flow resistance, which increases the energetic costs for pumping fluids through such channels. There is no a clear way to relate the fluid slip to the shear regime, since the distance depends on the sliding velocity as well as the liquid response to the shear applied to it by that motion. Previous studies<sup>17</sup> have shown the contact angle and the slip distance to have a strong but different functional dependences on the solid–liquid interaction potential. The contact angles have been found to decrease with the commensurability of size and packing between the fluid and the solid surface,<sup>26</sup> whereas the slip distance increases when the solid–liquid interaction becomes more repulsive.<sup>20</sup> All calculated slip lengths are relatively small, which is consistent with the favorable solid–liquid interaction found for all the liquids studied.

Figure 10 shows the velocity gradient for all liquids in the high shear regime. All liquids display a nonlinear velocity

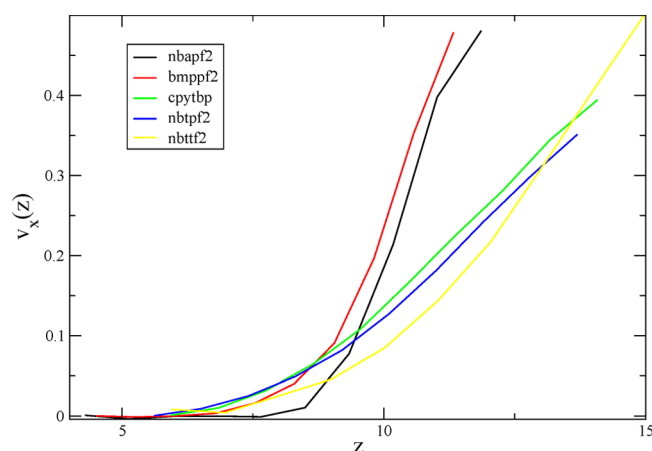


**Figure 10.** Thixotropic behavior observed for all liquids.

gradient under these flow conditions. The nonlinearity of the velocity gradient indicates a variable viscosity. This dependence of the viscosity on the shear rate is due to the influence of the flow on the structure of the liquid. All liquids studied exhibited a non-Newtonian thixotropic behavior as demonstrated by the upward concave shape of the velocity gradient. This behavior suggests a possible loss of structural isotropy as the liquid flows—a behavior typical of macromolecular liquids such as polymeric solutions and melts. In the case of ionic liquids, the behavior is more complex due to the strong electrostatic interaction between nonspherical ions with uneven charge distributions.

The functional relationship between the shear stress ( $\tau$ ) and the shear rate ( $\dot{\gamma}$ ), for a particular fluid, can be determined experimentally from viscometric flow measurements. This relationship is known as the *flow curve* for the fluid, and it has the form

$$\mu = \frac{\tau}{\dot{\gamma}} = m\dot{\gamma}^n \quad (8)$$

where  $m$  and  $n$  are the consistency and power-law indices, respectively. The flow curves for the ionic liquids studied here have been determined by calculating the local stress tensor and velocity gradient (shear stress) for the individual liquid layers (Figure 1). Table 5 shows the consistency and power-law

**Table 5.** Power Law and Consistency Indices for the Ionic Liquids

liquid	$m$ (Pa·s $^{n-1}$ )	$n$
[bmp][pf <sub>6</sub> ]	$(3196.0 \pm 0.0120) \times 10^4$	$1.0233 \pm 0.4711$
[cpy][tbp]	$(10.96 \pm 0.25) \times 10^2$	$0.6445 \pm 1.0261$
[nba][pf <sub>6</sub> ]	$2.560 \pm 9.677$	$0.4063 \pm 0.5241$
[nbt][pf <sub>6</sub> ]	$(1.729 \pm 232.3) \times 10^{-3}$	$0.0543 \pm 0.9571$
[nbt][tf <sub>3</sub> ]	$(28.214 \pm 0.357) \times 10^2$	$0.6556 \pm 1.4418$

indices for all liquids. The uncertainty in the values is mainly statistical and can be lowered by increasing the size of the system. The magnitude of the power-law index ( $n < 1$ ) indicates that these liquids follow the Ostwald power-law model<sup>21</sup> which represents accurately the shear thinning behavior of the fluid.

## CONCLUDING REMARKS

We have implemented a fully phenomenological approach to calculate the wetting and transport properties of ionic liquids. All ionic liquids studied exhibited good surface-wetting properties on silica, as demonstrated by surface contact angles with values far below 90°. The magnitude of the surface contact angles does not appear to depend on the crystallographic direction in which the liquid is propagating or receding. Despite their complexity, ionic liquids behave similarly to simple liquids when interacting with a solid surface. The liquid–solid interaction induces some structuring in the liquid near the solid–liquid interface. This structuring effect is dissipated on going into the bulk of the liquid.

The tribological simulations revealed three flow regimes: Newtonian, non-Newtonian, and oversheared. In the non-Newtonian regime, the ionic liquids displayed a thixotropic behavior, and their flow curves follow the Ostwald power-law model. They appear to thin as the applied shear increases, and despite the strong intermolecular interactions present in these liquids, the order parameter values seem to indicate some molecular orientation in the liquids as they flow.

The phenomenological approach used here allowed for the calculation of the liquids' viscosities with the appropriate accuracy and without the use of any calculational artifacts. Results support previous reports indicating that nonequilibrium techniques represent a more robust approach to the calculation of transport properties than do equilibrium methods based on time-correlation functions.

## AUTHOR INFORMATION

### Corresponding Author

\*E-mail henry.castejon@wilkes.edu (H.J.C.).

### Notes

The authors declare no competing financial interest.

## ACKNOWLEDGMENTS

Support for this work was provided by the National Science Foundation under Grant CHE-1012796.

## REFERENCES

- (1) Zaretsky, E. V. Liquid Lubrication in Space. *Tribol. Int.* **1990**, *23*, 74–93.
- (2) Liu, W.; Ye, C.; Gong, Q.; Wang, H.; Wang, P. Tribological Performance of Room-Temperature Ionic Liquids as Lubricants. *Tribol. Lett.* **2002**, *13*, 81–85.
- (3) Gunze, M. Driven Liquids. *Science* **1999**, *283*, 41–42.
- (4) Lipowsky, R. Morphological Wetting Transitions at Chemically Structured Surfaces. *Curr. Opin. Colloid Interface Sci.* **2001**, *6*, 40–48.
- (5) Young, T. An Essay on the Cohesion of Fluids. *Philos. Trans. R. Soc.* **1805**, *95*, 65–87.
- (6) Tadmor, R. Line Energy and the Relation between Advancing, Receding and Young Contact Angles. *Langmuir* **2004**, *20*, 7659–7664.
- (7) Cruz-Chu, E. R.; Aksimentiev, A.; Schulten, K. Water-Silica Force Field for Simulating Nanodevices. *J. Phys. Chem. B* **2006**, *100*, 21497–21508.
- (8) Deen, W. M. *Analysis of Transport Phenomena*; Oxford University Press: New York, 1998.
- (9) Bird, R. B.; Stewart, W. E.; Lightfoot, E. N. *Transport Phenomena*, 2nd ed.; John Wiley & Sons Inc.: New York, 2002.
- (10) Soong, C. Y.; Yen, T. H.; Tzeng, P. Y. Molecular Dynamics Simulation of Nanochannel Flows with Effects of Wall Lattice-fluid Interactions. *Phys. Rev. E* **2007**, *76*, 036303(14).



- (11) Tenney, C. M.; Maginn, E. J. Limitations and Recommendations for the Calculation of Shear Viscosity Using Reverse Nonequilibrium Molecular Dynamics. *J. Chem. Phys.* **2010**, *132*, 014103(8).
- (12) Hess, B.; Kutzner, C.; van der Spoel, D.; Lindahl, E. Gromacs 4: Algorithms for Highly Efficient, Load-balanced, and Scalable Molecular Simulation. *J. Chem. Theory Comput.* **2008**, 435–447.
- (13) Iler, R. K. *The Chemistry of Silica: Solubility, Polymerization, Colloid and Surface Properties, and Biochemistry*; Wiley: New York, 1979.
- (14) Lopez, P. E. M.; Murashov, V.; Tazi, M.; Demchuk, E.; MacKerell, A. D., Jr. Development of an Empirical Force Field for Silica. Application to the Quartz-Water Interface. *J. Phys. Chem. B* **2006**, *110*, 2782–2792.
- (15) Liu, H.; Maginn, E.; Visser, A. E.; Bridges, N. J.; Fox, E. B. Thermal and Transport Properties of Six Ionic Liquids: An Experimental and Molecular Dynamics Study. *Ind. Eng. Chem. Res.* **2012**, *51*, 7242–7254.
- (16) Wu, H.; Shah, J. K.; Tenney, C. M.; Rosch, T. W.; Maginn, E. J. Structure and Dynamics of Neat and CO<sub>2</sub>-reacted Ionic Liquid Tetrabutylphosphonium 2-cyanopyrrolide. *Ind. Eng. Chem. Res.* **2011**, *50*, 8983–8993.
- (17) Voronov, R. S.; Papavassiliou, D. V.; Lee, L. L. Boundary Slip and Wetting Properties of Interfaces: Correlation of the Contact Angle with the Slip Length. *J. Chem. Phys.* **2006**, *124* (20), 204701.
- (18) Monk, J.; Singh, R.; Hung, F. R. Effects of Pore Size and Pore Loading on the Properties of Ionic Liquids Confined Inside Nanoporous CMK-3 Carbon Materials. *J. Phys. Chem. C* **2011**, *115*, 3034–3042.
- (19) Voronov, R. S.; Papavassiliou, D. V.; Lee, L. L. Slip Length and Contact Angle over Hydrophobic Surfaces. *Chem. Phys. Lett.* **2007**, *441*, 273–276.
- (20) Thompson, P. A.; Robbins, M. O. Shear Flow Near Solids: Epitaxial Order and Flow Boundary Conditions. *Phys. Rev. A* **1990**, *41* (12), 6830–6837.
- (21) Osswald, T. A.; Menges, G. *Materials Science of Polymers for Engineers*, 3rd ed.; Hanser Publications: Cincinnati, OH, 2012.
- (22) Jiang, W.; Yan, T.; Wang, Y.; Voth, G. A. Molecular Dynamics Simulation of the Energetic Room-Temperature Ionic Liquid, 1-Hydroxyethyl-4-amino-1,2,4-triazolium nitrate (HEATN). *J. Phys. Chem. B* **2008**, *112*, 3121–3131.
- (23) Borodin, O. Polarizable Force Field Development and Molecular Dynamics Simulations of Ionic Liquids. *J. Phys. Chem. B* **2009**, *113*, 11463–11478.
- (24) Hu, Z.; Margulis, C. J. On the Response of an Ionic Liquid to External Perturbations and the Calculation of Shear Viscosity. *J. Phys. Chem. B* **2007**, *111*, 4705–4714.
- (25) Thompson, P. A.; Troian, S. M. A General Boundary Condition for Liquid Flow at Solid Surfaces. *Nature (London)* **1997**, *389*, 360–362.
- (26) Nijmeijer, M. J. P.; Bruin, C.; Bakker, C. F.; Van Leeuwen, J. M. J. A Visual Measurement of Contact Angles in a Molecular-Dynamics Simulation. *Physica A* **1989**, *160*, 166–180.